Upscaling the contribution of crab burrows to mangrove ecosystem functioning in French Guiana (South America)

Emma Michaud, Adelaide Aschenbroich, Thomas Stieglitz, Guillaume Brunier, Edward Anthony, Robert Curwood Aller, Gérard Thouzeau, François Fromard

Regional Environmental Change (2024) 24:165
https://doi.org/10.1007/s10113-024-02319-z

ORIGINAL ARTICLE

Upscaling the contribution of crab burrows to mangrove ecosystem functioning in French Guiana (South America)

Emma Michaud[1] · Adelaide Aschenbroich[1] · Thomas Stieglitz[2,3] · Guillaume Brunier[2,4] · Robert Curwood Aller[5] · Edward Anthony[2] · François Fromard[6] · Gérard Thouzeau[1]

Received: 4 June 2023 / Accepted: 20 September 2024

Abstract

Burrow characteristics and bioturbation activities of benthic organisms play a key role in mangrove ecosystem biogeochemical and sedimentary functioning. In this study, we aimed to understand how small-scale topographic variations in a mud bank might influence burrow morphology and distribution in a French Guiana pioneer mangrove system (Sinnamary estuary), and to upscale spatial patterns using remote sensing. We used burrow resin casting and sediment conductivity measurements to depict subsurface 3D burrow structures. We found that the spatial heterogeneity of burrow sizes (small, medium, large) and morphologies (simple I- and J-shape, complex geometries) depended on the geomorphic units within mudflats (platform, channel, depression). The aperture areas of burrow casts were used to predict the volume and complexity of each burrow type, enabling us to use drone-derived burrow opening distribution maps to calculate burrow volumes and complexity at the mudflat scale. There are clear associations between tidal channels and depressions and voluminous, multi-aperture, complex and multi-species burrows. In contrast, simple I- and J-shaped burrows inhabited by single species were mainly found on platforms. These relationships lead to a comparatively large volume of tidal-irrigated and deeply aerated sediments connected to channels and depressions compared to platform areas. We suggest that, depending on their morphology and connectivity with the topography, burrows may exhibit differences in biogeochemical functioning depending on the geomorphic unit. We warn against generalizing the functioning of mangrove ecosystems across geomorphic units where impacts may differ. Further studies are needed to understand how different burrow morphologies and life cycles may alter hydrological, sedimentary and biogeochemical functioning.

Keywords Amazon mud banks · Bioturbation · Burrow morphology · Drone imagery · Pioneer mangrove

Introduction

Mangroves, among the world's most productive ecosystems, are efficient at storing blue carbon in their sediments (Mcleod et al. 2011). Benthic organisms play a key role in the processing of organic matter (OM) through bioturbation activities, that help structure and promote microbial mineralization pathways (Booth et al. 2023, for review). In this regard, wetland crabs are ecosystem engineers, due to their burrow-dwelling behaviour, which modifies biogeochemical elemental cycles (Kristensen 2008; Agusto et al. 2022; Nie et al. 2021; Xi et al. 2023), hydrological processes (Stieglitz et al. 2013; Guimond et al. 2020) and local geomorphic patterns (Escapa et al. 2008; Needham et al. 2013). A recent study (Kristensen et al. 2022) concluded that mangrove carbon budgets should consider crab burrows in order to avoid underestimating carbon export, enabling a more accurate quantification of mangrove ecosystem processes and sinks or sources of major elements at both local and regional scales (Friess et al. 2022).

Although recognized as important, the contributions of processes associated with crab burrows (e.g. excavation, passive or active ventilation, diffusion) to carbon, nutrient and sediment budgets remain poorly quantified, due to difficulties in characterizing burrow volumes, surface areas and matter fluxes at the mudflat scale, and in evaluating possible

Communicated by Philippe Cuny and accepted by Topical Collection Chief Editor Christopher Reyer.

This article is part of the Topical Collection on *The highly dynamic French Guiana littoral under Amazon influence: the last decade of multidisciplinary research.*

Extended author information available on the last page of the article

species-specific differences. Natural patchiness hinders efficient characterization of burrow distribution at the mudflat scale. Patchiness depends on spatio-temporal variations of environmental parameters (sediment elevation, grain size, tidal range, vegetation structure, seasons…) and on crab species, size and behaviour (Wunderlich and Pinheiro 2013; Li et al. 2018). Egawa et al. (2021) showed that burrow density, proportion of renewed and collapsed burrows, and burrow depth and aperture were strongly correlated with distance from a tidal drainage channel, vegetation cover and organic matter content. Burrow shapes (e.g. large/complex and small/simple) also depend on sediment characteristics, vegetation cover, tidal gradient (Morrisey et al. 1999; Wang et al. 2014) and brachyuran crab families (i.e. Sesarmidae and Ocypodidae; Kristensen 2008; Min and Kathiresan 2021), all of which impact the sediment interfaces differently (Agusto et al. 2021). Single species may also have different burrow morphologies depending on sediment type (Katrak et al. 2008; Needham et al. 2010). Variations in crab behaviour in burrows can further lead to modifications of burrow volume and complexity, thus altering the effect on biogeochemical processes (Needham et al. 2011; Araújo et al. 2012). Evaluations of burrow volumes and morphologies associated with different stages of mangrove development are thus important steps towards a better understanding of the role played by the benthic fauna in the biogeochemical functioning of mangrove ecosystems.

The spatial and temporal dynamics of mangroves are particularly pronounced in environments with high mud inputs, such as the Guiana coast downstream of the Amazon River mouths. Mangroves along the French Guiana coastline (FG hereafter) rapidly colonize the highly mobile mud banks originating from the fine-grained sediment discharge from the Amazon River (Proisy et al. 2009). The pioneer stage of mangrove development is a critical phase of succession, which determines the plants'—and ultimately the ecosystem's—successful establishment. The processes involved in the functioning of pioneer mangroves therefore deserve more attention. Pioneer mangrove ecosystems are characterized by biogeomorphic variability on a centimetre to metre scale (Anthony et al. 2010; Brunier et al. 2016) with various geomorphic units, notably depressions (standing water at low tide) and tidal channel networks, which cross tidal flats (platforms). In FG, bioturbation by the dominant mangrove burrowing crab species (Ocypodidae and Ucididae) is spatially variable and difficult to accurately extrapolate over large areas (e.g. > 5 m^2; Aschenbroich et al. 2016). An exploratory survey by drone photogrammetry enabled, for the first time, the visualization of spatial heterogeneity of the distribution of burrow apertures at the mudflat scale (> 500 m^2; Brunier et al. 2020), illustrating that density of burrow openings depends on the geomorphic units, such as depressions and channels.

In the current study, we hypothesize that the presence of tidal channels, depressions and platforms in a pioneer mangrove drives changes in subsurface burrow morphology, and that their large-scale patterns can be estimated using remote sensing. In this framework, we aimed at (i) identifying and describing how small-scale topographic variations (i.e. tidal channels, depressions and platforms) influence burrow distribution and morphology in a pioneer mangrove system, and (ii) upscaling the spatial heterogeneity measured at ~ 1–10 m^2 to mudflat scales (100–1000 m^2) using drone technology.

Materials and methods

Study sites

Two pioneer mangrove systems located in the mouth of the Sinnamary River in French Guiana (5°28′42″N–53°2′1″W and 5°28′39″N–53°0′2″W, respectively; Fig. 1a, b) were studied at low spring tide in the dry season (August to December) during three consecutive years. In November 2013, we only investigated site A, covering 0.25 km^2. The relative contribution of the total pioneer mangrove area was estimated at 10.3% from the analysis of very high-resolution aerial photos (27 × 27 cm; 2013/11/07; Fig. 1c). In October 2014 and September 2015, site A was no longer accessible due to mud accumulation in the western part of the mouth of the Sinnamary River. A second site, B (0.59 km^2), was therefore investigated (Fig. 1d) in 2014 and 2015. Site B showed three substrate consolidation states: (1) water-saturated mud recently deposited during low tide exhibiting a very smooth surface, (2) consolidated mud assimilated with platforms, drained at low tide by channels and characterized by numerous depressions, and (3) consolidated bare mud with patchy colonization by mangrove trees of varying ages and sizes (Brunier et al. 2020). Colonization typically resulted in the establishment of a fringe of young mangroves (~ 0.5–1 m height) within a few months.

Both sites experience semi-diurnal tides and were submerged at each tide during spring tides. They were located at neap and spring high-tide water levels of 2.8 m and 3.2 m above mean sea level, respectively. At low tide, the water levels during neap and spring tides ranged between 1.3 ± 0.3 and 2.1 ± 0.3 m, respectively. Drainage channels examined in this study were generally less than 1 m wide. At both sites, the highest part of the mud bank colonized by mangroves (e.g. platform) was flooded for 3 to 4 h only during high spring tides, while the channels and depressions were flooded for 5 to 8 h depending on depth (Brunier et al. 2020; Michaud et al. 2022). Platform flooding was more variable during neap tides, from less than 1 to 3 h in the eastern sector and 3–5 h in the central sector, which is regularly intersected by channels and depressions, and 2–4 h on the remaining platform.

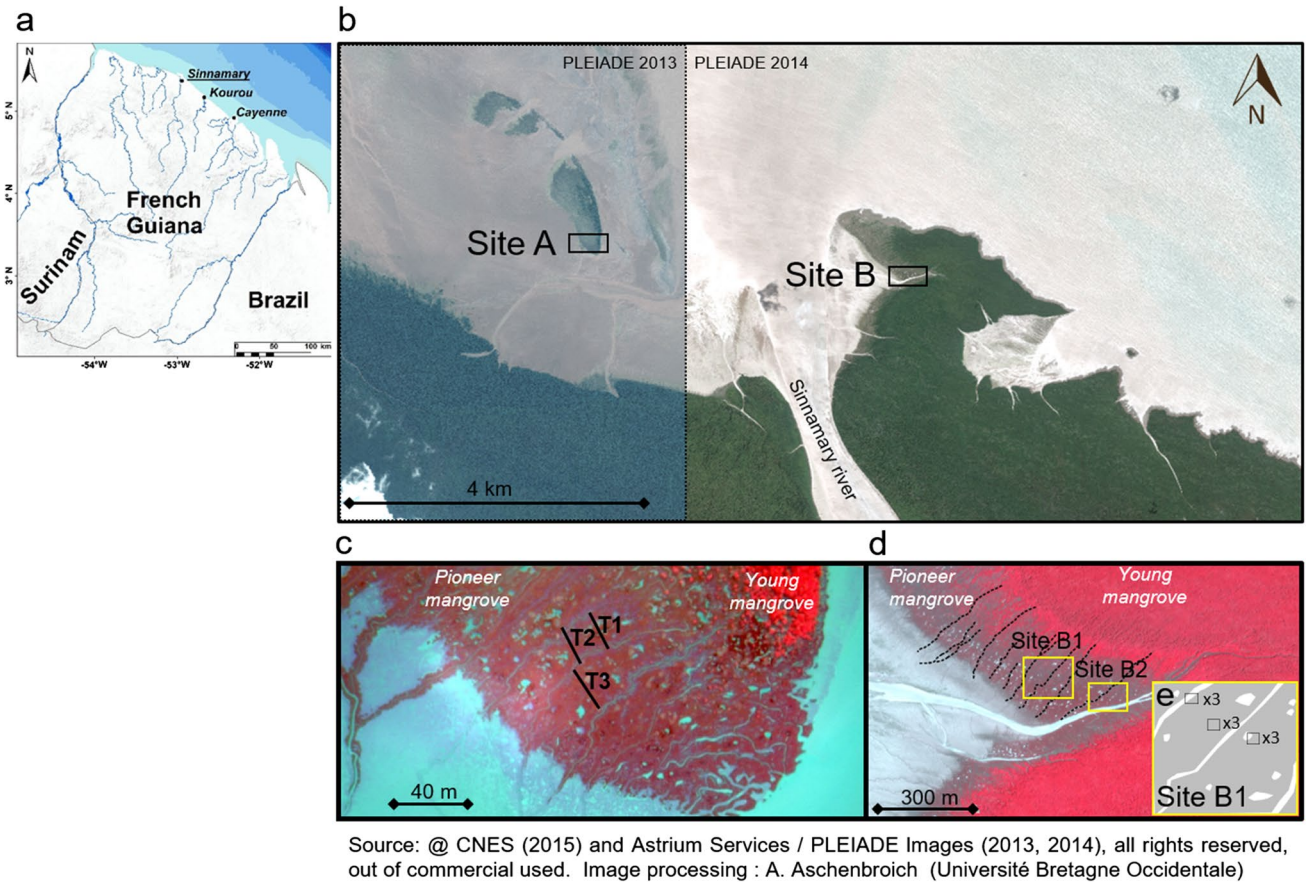

Fig. 1 **a**) General map of the French Guiana located in South America. **b**) Satellite images (PLEIADE) showing the site A in 2013 and site B in 2014, both of them are located at the mouth of the Sinnamary estuary in French Guiana. **c**) Site A: aerial photograph with transect (T) locations in 2013 (T1: 20 m; T2: 21 m; T3: 27 m). **d**) Site B: satellite image showing location of the site B1 studied in 2014 and the site B2 whose the aerial UAV survey carried out in 2015. The depressions and tidal channel network is represented by the doted lines. **e**) Sketch map of Site B1 showing the three geomorphic units investigated (Channels (CH), Platform (PF) and Depressions (D)) in three replicates each (× 3), for the study of burrow aperture distribution in October 2014.

Sampling

Counting of burrow apertures

In 2013 (Nov 7), three transects were positioned between two channels at site A at the same tidal level (Fig. 1c). The transects were 20, 21 and 27 m long (Fig. 1c). Each transect covered the three geomorphic units (GU) platforms, channels and depressions. Along each transect, we investigated quadrats every metre, i.e. 20, 21 and 27 quadrats for transects 1, 2 and 3, respectively. In 2014 (Nov 4–8), we randomly investigated three replicated quadrats (1 m^2) per geomorphic unit (platforms, channels and depressions) at the same tidal level at site B (Fig. 1d, e) to document burrow distribution patterns within each unit (Aschenbroich et al. 2016). In 2015 (Sept 29–Oct 3), site B was revisited (Fig. 1d) using a drone that took a series of aerial photographs at very high spatial resolution (0.5 cm per pixel), enabling a detailed survey of burrow apertures (BO) and their relation with geomorphic features (Brunier et al. 2020).

All visible burrow apertures were counted, and their average diameters were measured to the nearest millimetre within each quadrat. Burrow apertures were approximately circles, and we assigned each a circular diameter. Three size classes were defined as small BO ($Ø < 2$ cm), medium BO ($2 \le Ø \le 5$ cm) and large BO ($Ø > 5$ cm), according to the body size structure measured for the whole crab community in this area (Aschenbroich et al. 2016). Small and medium aperture sizes were mainly attributed to *Uca cumulanta* and *Uca maracoani*, respectively. Large aperture sizes could not, however, be attributed to *Ucides cordatus*, as measured by Aschenbroich et al. (2016) in the young forest, because this species did not occur in the pioneer mangrove stage. The total burrow aperture area (AA, in cm^2) was calculated as $AA = \sum_{i=1}^{n} \pi (\frac{1}{2} Ø_i)^2$, where n is the number of burrow apertures and $Ø_i$ the aperture diameter of the i^{th} burrow (in cm).

Burrow morphology

Conductivity profiles Burrow subsurface morphology was explored at site B in 2014 (24–27 Oct) by first using a specially designed half-Wenner conductivity sensor for subsurface apparent electrical conductivity. This method identifies bioturbated cavities in the sediments because the water in the burrows has a higher conductivity than the bulk sediment (Stieglitz et al. 2000b). Vertical conductivity profiles were recorded near tidal depressions and channels, along three transects 1.5 to 3 m long, both perpendicular and tangential to microhabitats (Fig. 3a). The profiles were spaced ca. 20 cm apart, at a total of 7–10 profiles per transect. For each profile, the electrode was vertically introduced within the sediments and conductivity recorded every 2.5 cm up to 25 cm depth, and every 5 cm until 1 m depth. The sensor measures the apparent bulk conductivity of sediment in a sphere of approx. 4 cm diameter around the electrode. For each vertical profile, total conductivity along a given vertical profile (C_{total} in mS cm^{-1}) was calculated as:

$$C_{total} = a \times C_{burrow\ water} + (1 - a) \times C_{sediment} \quad (1)$$

where a is the proportion of burrows per volume of sediment, and $C_{burrow\ water}$ and $C_{sediment}$ represent the burrow water and non-bioturbated sediment conductivity (mS cm^{-1}), respectively.

Typical C_{total} conductivity was 15.04 to 17.69 mS cm^{-1} vs. 13 mS cm^{-1} for $C_{sediment}$ and 55 mS cm^{-1} for burrow water (calculated from (measured) salinity of 32.5 and temperature of 30 °C). Conductivity ranges were interpreted as follows: < 15 mS cm^{-1} representing non-bioturbated sediment, 15–18 mS cm^{-1} suggesting small burrow galleries, and > 18 mS cm^{-1} indicating major burrow chambers filled with seawater. In these calculations, we assumed that sediment porosity was constant and that pore water salinity was the same as burrow water salinity.

The proportion of burrows per volume of sediment, a, was estimated as:

$$a = \frac{C_{total} - C_{sediment}}{C_{burrow\ water} - C_{sediment}} \quad (2)$$

In order to normalize the burrow volume (V_{bur}) to a volumetric sediment unit of 1m^3 (L m^{-3}), we used:

$$V_{bur} = a \times S_u \times D_{bur} \quad (3)$$

with a the fractional proportion of burrows, S_u the sediment surface unit of 1 m^2, and D_{bur} (m) the maximum burrow depth under the sediment surface identified with the conductivity profiles.

Resin casting Burrow morphology (volume, depth and complexity) associated with each BO size class was further investigated in each geomorphic unit at site B using resin casts (Stieglitz et al. 2000a) (Oct 24–27, 2014). Burrows were selected at a comparable tidal level to exclude a potential shore height effect on burrow morphology. Burrows were filled with polyester resin (@crystic 115NA) at low tide. The addition of 0.5% of peroxide catalyst (@ Butanox M50) was sufficient to allow the resin to set before the next tide. Casts were excavated manually after 24 h. The number of BO per resin cast was counted, their diameters measured and the total burrow aperture areas calculated. When multiple apertures were counted for a single resin cast, we added up the area of all associated apertures. We distinguished burrow length (L_{bur}, cm), considered the sum of all lengths of the different parts of each resin cast, and burrow depth, which corresponded to the distance between the burrow aperture (at the sediment surface) and the deepest point of the cast, thereby assuming that the resin completely filled the individual burrow systems. Burrow volumes (V_{bur}) were estimated by immersing cleaned casts in water-filled graduated containers (mm). Burrow complexity was assessed by the number of intersections (C_x) between burrow galleries. Large macrofauna trapped in the resin casts or observed or collected by hand in the sediment during cast excavation were identified when possible. In order to allow meaningful comparisons of burrow architecture between geomorphic units, we estimated the burrow volume and complexity per unit area (m^2). We used linear regressions to predict the burrow volumes and complexity (BV m^{-2} and C_x m^{-2}) from the burrow aperture area (AA cm^2) for each plot investigated.

Data analyses

Burrow counting

At site A, the GU influence (platform, channel, depression) along transects on BO density and aperture area per BO size class was tested using a nested PERMutation ANalysis Of VAriance (PERMANOVA) with 999 permutations and $\alpha = 0.05$ (Underwood et al. 2004; Anderson 2017). Correlation analyses were used to quantify the relatedness among the densities and surface areas of the different BO size classes with non-parametric Spearman multi-correlation analysis.

At site B, the same number of replicates per GU positioned at random and non-parametric data led us to perform a PERMANOVA with 999 permutations and $\alpha = 0.05$ to test the effects of GU (channel, depression, platform), BO size classes (small, medium, large) and their interactions (GU × BO size class) on burrow density and aperture area. Pairwise permutation tests were used as post hoc tests.

Burrow morphology

The relatedness among burrow features was quantified with non-parametric Spearman multi-correlation analysis. To determine which parameters of burrow geometry (number of apertures, aperture area, total length, depth, volume, complexity) explained the largest variability among GU (platform, channel, depression), a principal component analysis (PCA) was performed on the correlation matrix. Data were normalized prior to analysis. We tested the influence of GU on the overall parameters of burrow geometry by using a non-parametric one-way analysis of variance (Kruskal–Wallis test) followed by Wilcoxon tests (for pairwise comparisons).

In order to allow meaningful comparisons of burrow morphology between GU, we estimated the burrow volume and complexity per unit area (m^2). To this end, we explored the possibility that the aperture surface (cm^2) of burrow casts predicts burrow volume (BV) or complexity (C_x, number of intersections), using Pearson's linear regressions. When the linear relationships were significant ($p < 0.05$), we estimated burrow volume and complexity (BV m^{-2} and Cx m^{-2}) for each study plot based on the distribution of burrow apertures measured at site B in 2014. Then, after verifying the variance homogeneity, a parametric analysis of variance (ANOVA) was used to determine whether the three categories of GU had an effect on the mean volumes and complexities of the burrows in the plots.

All statistical analyses were performed within the R environment (R Development Core Team, 2021) using the vegan (Oksanen et al. 2020) and FactoMineR (Lê et al. 2008) packages, with the function "adonis2" for the nested Permanova analysis (Oksanen et al. 2020).

Burrow upscaling

The burrow aperture maps derived from UAV-based images (0.5 cm per pixel) (Brunier et al. 2020) were used to normalize total burrow volume in cm^3 (BV) and burrow complexity (C_x) metrics per m^2 from linear relationships calculated previously. Burrow aperture area, volume and complexity were computed on individual burrows using ESRI ArcGIS desktop 10.6.2. Using the GIS spatial joint function, these metrics summed into a fishnet polygon grid of 1×1 m (Brunier et al. 2020). The spatial occupation of burrows was calculated as BV divided by the total volume of the mudflat per unit area. Mudflat volume was derived from the UAV-based Structure from Motion Photogrammetry topographic end-product named Digital Surface Model (DSM). The DSM was generated with an average vertical accuracy of ± 5 cm and a resolution of 1 cm per pixel (Brunier et al. 2020). It was used to calculate the mudflat volume above an elevation of −0.75 m which was related to the tidal channel thalweg elevation.

Results

Burrow aperture distribution across the different geomorphic units

At site A in 2013, small, medium and large BO represented about 70%, 20% and 10% of the total number of BO, respectively. BO density and surface for each diameter class were similar across transects (Fig. 2). The geomorphic units (GU) impacted significantly BO variables for each size class (Fig. 2; $F_{(6,59)} = 5.40$, $p < 0.004$ and $F_{(6,59)} = 4.54$, $p < 0.013$, for S density and surface, respectively; $F_{(6,59)} = 3.24$, $p < 0.001$ and $F_{(6,59)} = 3.17$, $p < 0.003$, for M density and surface, respectively; $F_{(6,59)} = 6.76$, $p < 0.001$ and $F_{(6,59)} = 6.54$, $p < 0.001$, for L density and surface, respectively). Despite higher densities along each transect, small BO made the smallest contribution to total BO surface, typically ~ 1–10 cm^{-2} m^{-2} (Fig. 2b). The density and surface area of small BO did not vary significantly between GU, whereas BO density and surface area of medium and large BO did (pairwise.perm.t.test, $p < 0.05$), both having been significantly higher near channels and depressions (Fig. 2; pairwise.perm.t.test, $p < 0.05$). Densities and surface areas of medium BO were positively correlated with those of large BO ($\rho = 0.72$).

At site B in 2014, we observed a significant effect of size on BO density ($F_{(2,18)} = 47.06$, $p < 0.001$). In contrast, GU showed no significant effect on BO density ($F_{(2,18)} = 0.83$, $p > 0.55$), independently of size ($F_{(4,18)} = 0.51$, $p > 0.75$). Neither GU nor size had a significant impact on BO surface ($F_{(2,18)} = 1.26$, $p = 0.329$ for "GU"; $F_{(2,18)} = 0.91$, $p = 0.513$ for "size"). The interaction between "GU" and "size" was also not significant ($F_{(4,18)} = 1.06$, $p = 0.433$).

Burrow morphology associated with large burrow apertures

Smaller galleries and larger excavation chambers differed from "unexcavated" sediments by their comparatively higher bulk conductivity (Fig. 3). Typical sediment conductivity below 40 cm depth and away from the depressions and channels was 13.3 ± 0.7 mS cm^{-1} (Fig. 3b). Bulk sediment conductivity > 15 mS cm^{-1} was detected until ca. 25 cm depth all along transect 1 tangential to the depression (profiles 1–7), on transect 2 across the depression (i.e. profiles 3–7) and on transect 3 perpendicular to the depression (i.e. profiles 2–7; Fig. 3b). This range of conductivity suggested sediments bioturbated by small galleries. Conductivity values > 18 mS cm^{-1}, suggesting larger burrow chambers, were mainly detected in the interior of each

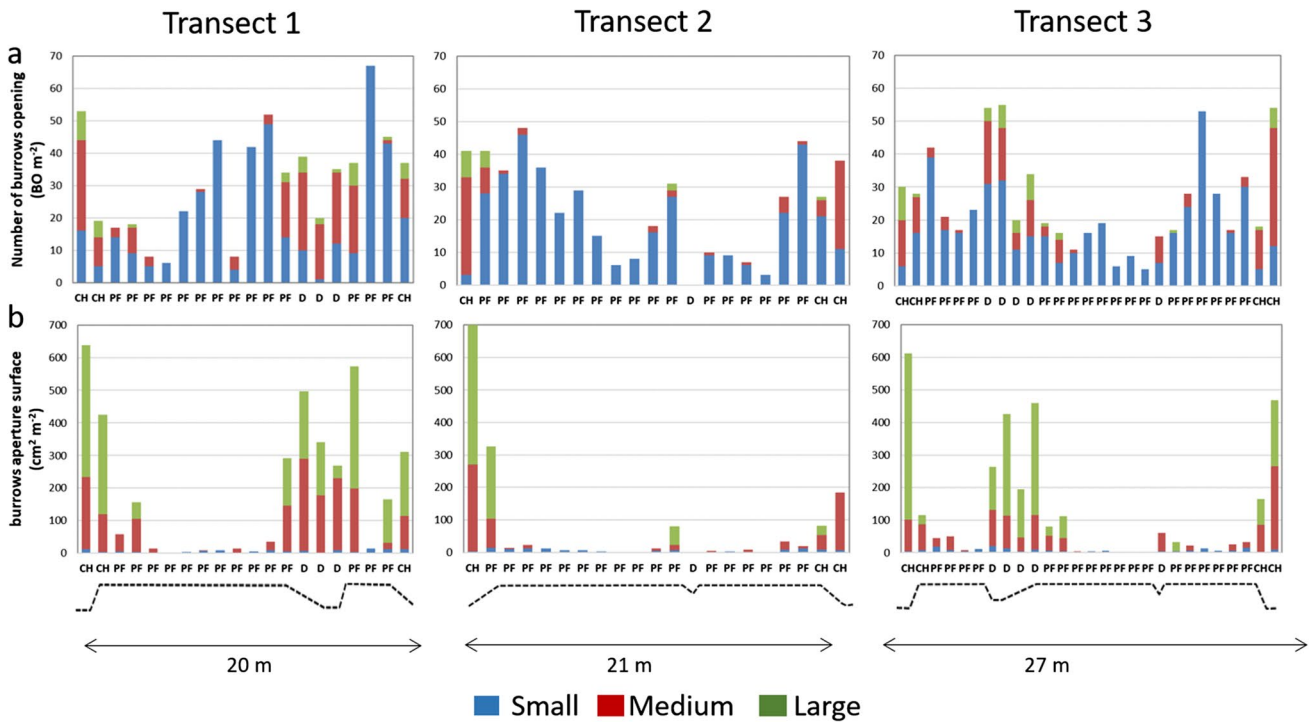

Fig. 2 Site A investigated in November 2013. (**a**) Density of burrow apertures (BO m^{-2}) in plots along the transects for each size class (T1: 20 m; T2: 21 m; T3: 27 m). (**b**) Standardized total burrow aperture area (cm^2 m^{-2}) for each size class. Schematic topographical profiles are shown below the graphs; CH, tidal channels; PF, platform; D, depressions

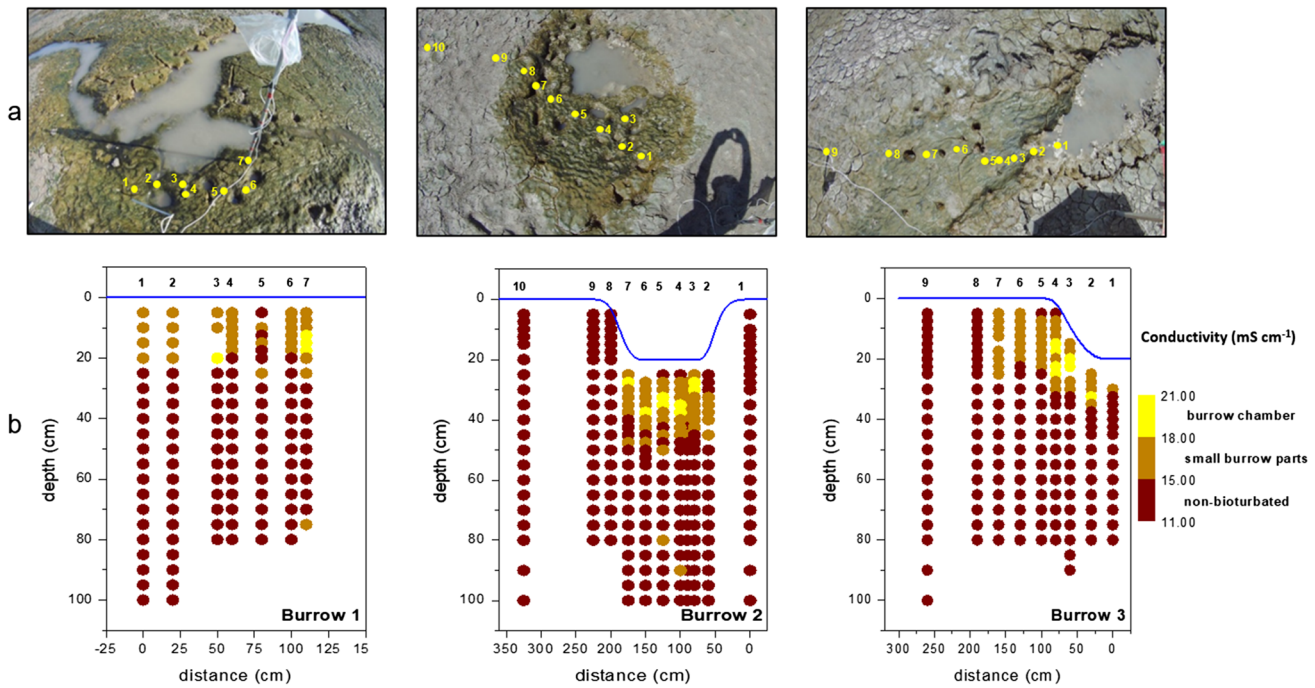

Fig. 3 Conductivity measurements at site B in 2014. Site B. (**a**) Location of conductivity transects around the depressions and tidal channels. Spots represent vertical conductivity profiles starting at the sediment surface. (**b**) Vertical profiles of conductivity (mS cm^{-1}) along transects. The conductivity values rise as increasing amounts of burrow water contribute to the volume of sediment measured; conductivity ranges were defined as < 15 mS cm^{-1} representing non – bioturbated sediment, 15–18 mS cm^{-1} suggesting small burrow galleries, and > 18 mS cm^{-1} indicating major burrow chambers filled with seawater

depression (transect 2, profiles 3–7; transect 3, profiles 2–4; Fig. 3b). The distribution of the highest conductivity value indicated that the bioturbated zone likely extended to ca. 25 cm below the surface. We did not detect high conductivity between 30 cm and 1 m depth in this area. On transect 3, the galleries extended 1.5 m away from the interior of the depression, but not beyond the burrow apertures, as the galleries (presumably) converged towards the depressions and tidal channels.

The fraction a of the overall burrow volume of 4.1 to 10.4% was therefore calculated for a median depth of 25–30 cm below the surface, which is equivalent to burrow volumes of 10 to 26 L m^{-3}.

Burrow morphology across different geomorphic units

The small BO, primarily located on the platform, were associated with single burrows ranging in length and volume from 5 to 30 cm, and from 2 to 123 cm^3, respectively, with no visible intersection (Fig. 4a). Medium BO were most commonly associated with simple J-shaped burrows (Fig. 4b), but also U-shaped burrows (Fig. 4b (2); $n = 1$), several galleries (from 2 to 19) sharing a single aperture (Fig. 4b), and complex burrows connected to both channels and depressions (Fig. 4b (4); $n = 2$). Length, volume and complexity of these burrows ranged from 24 to 100 cm, 160 to 7700 cm^3 and from 0 to 48 intersections, respectively. Large BO were mainly associated with multiple aperture burrows (Fig. 4c) connected to channels and depressions. These burrows ranged in length, volume and complexity from 122 to 165 cm, 8800 to 17,800 cm^3 and from 189 to 269 intersections, respectively. One large single-aperture burrow had a shorter length (30 cm) and a smaller volume (180 cm^3). Correlation analyses indicated significant relationships among all the burrow features based on the Spearman correlation coefficients ($p < 0.05$; online resource 1).

The PCA analysis explained 93% of the morphological variability of burrows among the geomorphic units, with the first component accounting for 74.4% and the second component accounting for 18.4% (Fig. 5). The main variables (and their loadings) defining the first axis were the burrow total aperture area (0.97), length (0.87), volume (0.98) and complexity (0.96), while burrow depth (0.93) defined the second axis (Fig. 5a). Burrows were separated into three groups of locations along the first component: depressions, channels and platforms (Fig. 5b). Burrows

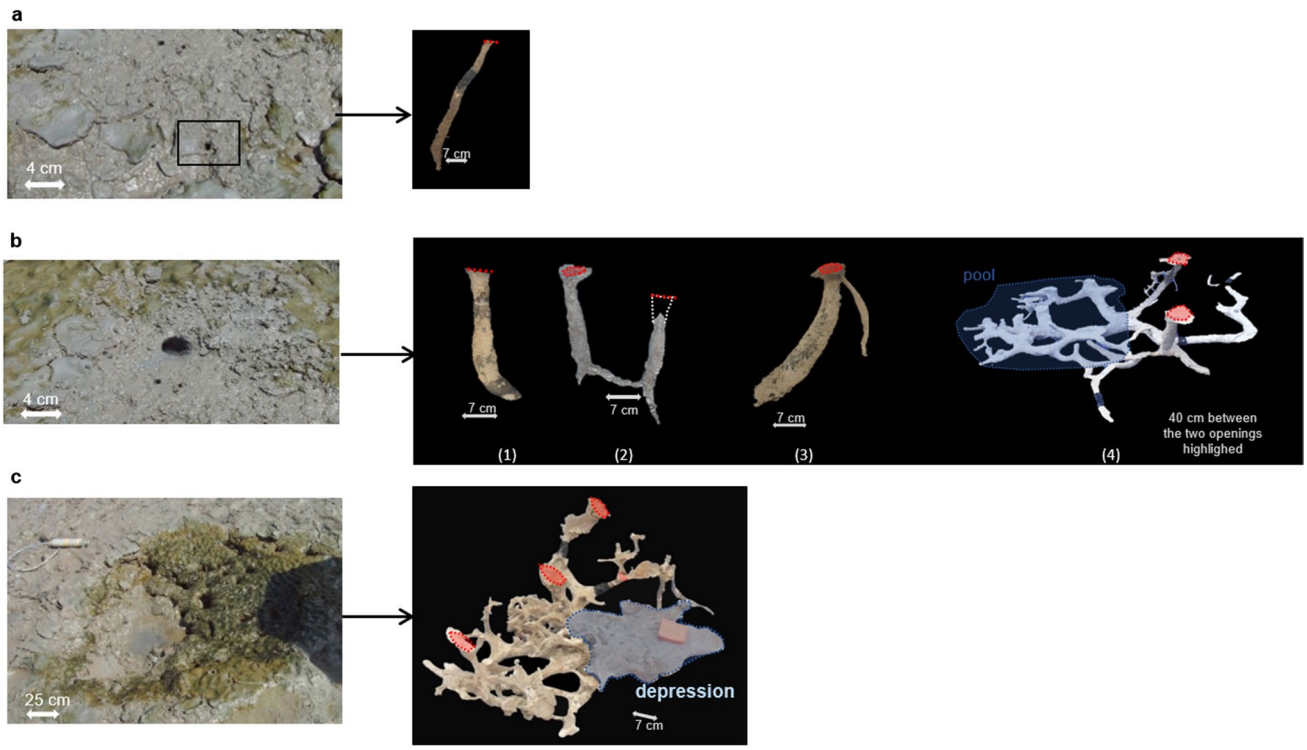

Fig. 4 Resin casts of burrow morphology for small, medium and large burrow apertures (BO) obtained at site B in 2014. (**a**) Small BO. (**b**) Medium BO showing (1) J-shaped, (2) U-shaped, (3) a single shared aperture and (4) complex burrow either associated with depression or tidal channel. (**c**) Large BO (only 2/3 of the burrow could be reconstructed). Burrow morphologies: red area or dotted lines refer to the apertures of main branches; blue areas locate surface depressions

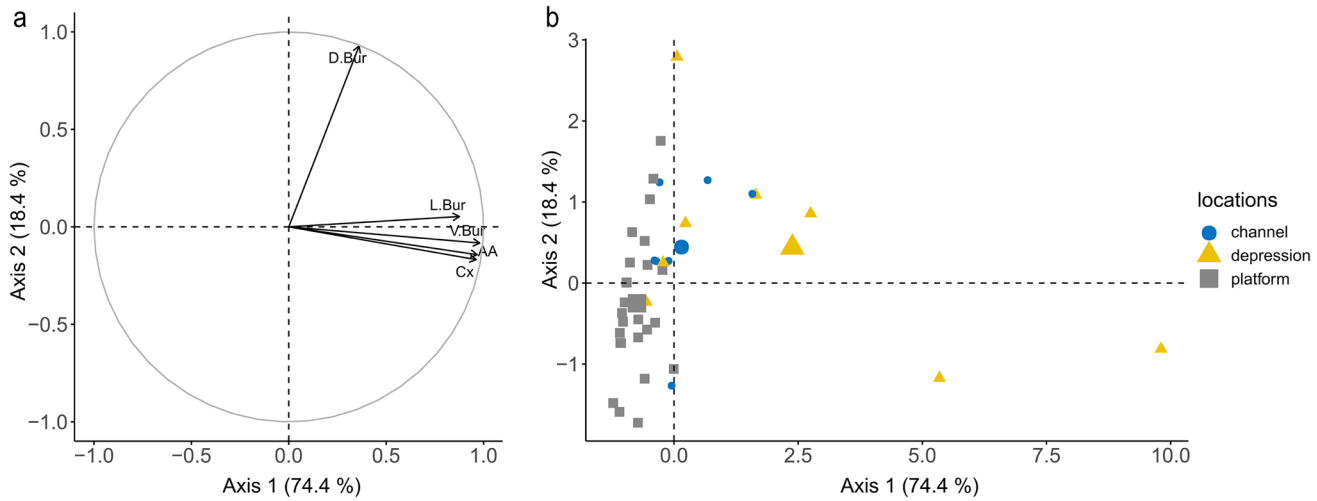

Fig. 5 **a**) The correlation circle for the Principal Component Analysis with burrow length (L_{Bur}), volume (V_{Bur}), complexity (C_x) and aperture area (AA) as explaining variables on the first axis and burrow depth (D_{bur}) as explaining variable on the second axis. The first two axes explain 93% of the variability in the data. **b**) Principal Component Analysis based on burrow geometry of each resin cast at different locations (channels, depressions and platform)

near or within depressions were characterized by the PCA as having the largest volume, complexity and length. A higher total burrow aperture area was associated with a greater number of apertures for the same burrow cast. In contrast, burrows on the platform exhibited the lowest volume and length and the least complexity. Burrows near channels were characterized by intermediate values of these parameters, and did not form a clearly distinct group. Burrow depth did not characterize any of the burrow groups. Overall, the burrow length, volume and complexity, as well as the burrow aperture area, were significantly higher near channels and depressions (KW, $p < 0.0005$), unlike burrow depth.

Despite the lack of quantitative data on the abundance and diversity of the infauna associated with each burrow cast, we observed that fiddler crabs, *Uca cumulanta*, inhabited small burrows. We identified larger fiddler crabs (*Uca maracaoni* and juveniles of *Uca* spp.) in medium BO casts. We also found other species during the excavation of the medium and large burrow casts: the swimming crab *Callinectes bocourti*, the grapsid *Goniopsis cruentata*, the goby *Gobionellus oceanicus* and the anguilliform *Myrophis* cf. *plumbeus*. Fish species were occasionally trapped in the secondary galleries connecting the inside part of the depressions and tidal channels to the main burrow branches. We observed that the latter were connected to channel and depression edges.

Burrow volume and complexity per unit surface area

Burrow volumes for each BO size class were significantly correlated with the burrow aperture areas of all resin casts for each BO size class ($BV_{small} = 0.09 \times AA$ with $R^2 = 0.34$ at $p < 0.02$; $BV_{medium} = 0.06 \times AA$ with $R^2 = 0.93$ at $p < 0.001$; $BV_{large} = 0.03 \times AA$ with $R^2 = 0.99$ at $p < 0.005$). Burrow complexity was significantly correlated with the burrow aperture areas of medium ($C_{xmedium} = 0.31 \times AA$; $R^2 = 0.43$, $p < 0.0004$) and large ($C_{xlarge} = 0.46 \times AA$; $R^2 = 0.95$, $p < 0.01$) BO, while the small BO were not complex.

In order to apply these equations to the burrow apertures counted on plots in 2014, the aperture areas considered in the equations did not include the burrow apertures within the deeper parts of tidal channels and depressions (they were not visible during the counting process). We do not think this to be a significant source of error, as only burrows casts connected to depressions and tidal channels were considered. Mean burrow volumes measured from the aperture areas in each plot were 9.95 ± 2.80 L m^{-2}, 6.7 ± 4 L m^{-2} and 4.5 ± 1.8 L m^{-2} for the depressions, channels and platform, respectively; they did not differ significantly (ANOVA, $F_{2,6} = 2.04$, $p > 0.2$; Online resource 2). Mean burrow complexity varied from 27 to 7 intersections m^{-2} depending on the geomorphic unit (Online resource 2). Although the largest burrow complexities were measured along the depressions, they did not differ significantly with the lower burrow complexity observed across the two other geomorphic units (ANOVA, $F_{2,6} = 1.50$, $p > 0.3$).

Upscaling of burrow characteristics

The total normalized burrow volumes (cm^3 per m^2), the burrowing spatial occupation (hereafter the volume balance in %)

and burrow complexity were mapped over the mudflat (Fig. 6). Burrow volumes ranged from 30 to 20,000 cm^3 m^{-2}, with the highest volumes being located near depressions and channels (Fig. 6a–b). Space occupation by burrowers ranged from 0.05 to 30% (Fig. 6b), with higher values in the lower part of the mudflat (> 2%), associated with small channels and depressions (Fig. 6a). The upper part of the mudflat was characterized by an average volume balance of 0.25%, except above the unconnected pools where it reached over 2% (Fig. 6c).

The platform (mudflat) hosted ~ 75% of total burrow volume (Online resource 3a), with the highest density of small burrows on its upper part. The remaining quarter of the total burrow volume was found on the edges of main and secondary channels (9% and 5.5%, respectively), and at the level of connected and unconnected depressions (8.6% and 1.1%, respectively).

Burrow complexity was consequently lower on the upper part of the mudflat (Fig. 6d), where single small galleries were dominant with a C_x median of 1.13, while step morphologies ranged from 2.41 to 3.88 (Online resource 3b). In contrast, burrow complexity was higher in the areas dominated by channels and depressions (Online resource 3b).

Discussion

Burrow morphology varies with species and geomorphic unit

Most fiddler crab species are known to regularly maintain their burrows: they prevent burrows from collapsing by closing their entrance with mud plugs during rising tides, and regularly excavate deeper sediment during low tides (Qureshi and Saher 2012; Machado et al. 2013). They also avoid burrowing into a fluid matrix, i.e. on lower-elevation substrates and inside the tidal channels or connected depressions, because this would increase the maintenance efforts (Lim 2006). Sediments on tidal channel banks, however, were sufficiently consolidated for burrowing activities, as observed elsewhere (Wang et al. 2009).

Small- and medium-sized burrows were numerically dominant at our study sites in 2013 and 2014. Brunier et al. (2020) calculated that small, medium and large size classes accounted for 55%, 39% and 6%, respectively, of the total number of burrow apertures at site B in 2015. They showed that small and medium densities increased from SW to NE,

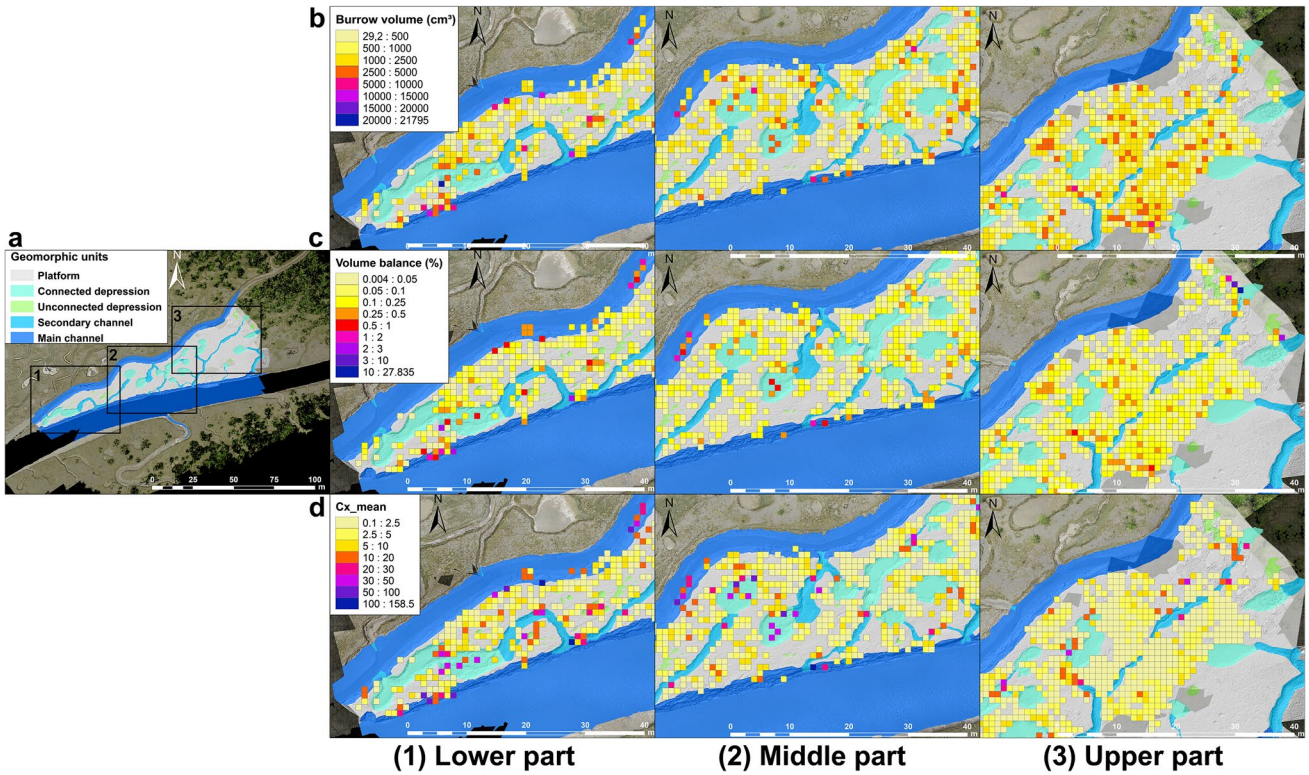

Fig. 6 **a**) Aerial UAV view of the study site in 2015 (site B2) showing the different geomorphic units (platform, connected and unconnected depression, secondary and main channels) for the three parts of the mudflat (lower (1), middle (2), upper (3) parts). **b**) Spatial distribution of burrow volumes in cm^3 m^{-2} for each part of the mudflat. **c**) Volume balance (i.e., burrowing spatial occupation in %) for each part of the mudflat. **d**) Average burrow complexity Cx m^{-2} for each part of the mudflat

where the mudflat was less incised by channels and depressions, and had a larger platform surface, a higher elevation (of 0.3 to 0.5 m) and slopes > 5°. On the contrary, large-sized burrows were abundant on steep slopes (up to 30°) on low-elevation features, which agrees with our observations along the channels and depressions in our 2013 and 2014 datasets. These authors highlighted that 60% of large burrows were associated with connected channel banks, and 5% with unconnected depressions. Small and medium class apertures were located less than 75 cm or 1 m apart, while large burrow class apertures were not clustered and were more than 3 m apart.

Based on our field observations and on another study in the same site (Aschenbroich et al. 2016), we suggest that burrows with small and medium apertures are inhabited by fiddler crab species, *Uca cumulanta* and *Uca maracoani*, which is consistent with their high density observed on the platform and their need to feed and defend their territory on the more elevated areas. We also note that the larger the individuals, the further apart are the burrows, due to territorial behaviour (Cannicci et al. 2018).

Uca burrows are generally single-aperture, simple-shaped and shallow. They are typical J-shaped or double-entry U-shaped burrows due to species specificity or in response to tidal level, vegetation and sediment characteristics (Lim and Diong 2003; Lim and Heng 2007; Qureshi and Saher 2012). In our study area, apertures shared between galleries and U-shaped burrows were primarily associated with the channel edges and the platform. Burrows may have been shared by several fiddler crab individuals or with smaller infauna, thereby providing new microhabitats for other organisms (Stieglitz et al. 2000a; Kristensen 2008). In two highly complex burrows with medium apertures located on depression edges, multiple second-order branches flatten out, converging inward from the main branches, towards standing water depressions (Fig. 4b). Given the small diameter of the secondary galleries, they may have been excavated by burrowing fish found in the casts (e.g. *G. oceanicus*, *M. plumbeus*, 5–10 cm length) or by shrimps (Henmi et al. 2017).

Previous studies have shown that very complex burrows with multiple apertures, resulting either from several burrowing generations or from multi-species constructions, are generally associated with grapsoid crab species (Stieglitz et al. 2000a; Needham et al. 2010). However, we observed only one grapsoid (*G. cruentata*, grapsid family) in our study, but several fiddler crab species (*U. maracoani*, *U. cumulanta*, *Uca* spp. juveniles) in the main burrow branches at the time of sampling. One of these complex burrows presented freshly excavated sediment around its entrance, demonstrating recent (fiddler) crab activity. As fiddler crab species generally avoid tidal flushing in their burrows, the presence of these species in these structures could have been only temporary during low tides, motivated by a search for food or shelter. Occupation time of crab burrows may have been shortened near to depressions/channels also due to burrowing activity of other channel species that enhance flooding from the burrow bottom.

Large apertures were also associated with large and highly complex burrows connected to standing water, but were not inhabited by burrowing crabs. Burrow apertures on the depression/tidal channel edges were not surrounded by excavated sediment, suggesting no recent activity in the burrows. A well-developed benthic biofilm on the margins of the tidal depressions and channels corroborates this, in addition reflecting the lack of grazing by fiddler crabs. By hindering substrate erosion (Austen et al. 1999; Decho 2000), biofilms are likely to prevent burrow infilling and/or destruction despite the absence of burrow maintenance activity by crabs. Other faunal organisms, such as burrowing fishes and shrimps, were observed in these burrows; their activity may contribute to burrow maintenance (Karpulus et al. 1972; Dinh et al. 2014; Henmi et al. 2017). Our experimental design did not allow identifying whether these burrows were initiated by fiddler crabs, and later abandoned as soon as they were connected to standing bodies of water, or directly created by the burrowing activity of fishes and shrimps. Because the highly complex and multi-species burrows were exclusively associated with tidal depressions and channels, we consider that these microhabitats promote burrow co-construction by diverse species and, in turn, hydrological connectivity between emerged edges and submerged tidal depressions and channels.

Overall, our data suggest that changes in burrow volume were rather due to lateral extension and interconnectivity than to deepening of burrows. Aperture types and geomorphic units were not determining factors controlling burrow depth. Generally, shore height determines burrow depth because the phreatic water level is sought by burrowers (Bortolus and Iribarne 1999). The depth of burrows in our study (6–40 cm depth) was comparable with that from other studies in salt marshes and mangroves (Bertness and Miller 1984; Lim 2006; Qureshi and Saher 2012; Machado et al. 2013; Dinh et al. 2014). It has been hypothesized that burrow depths of less than 50 cm, usually found in anoxic sediments, may improve burrow aeration by limiting the amount of accumulated stagnant air compared to deeper burrows (Lim and Diong 2003).

Potential burrow effect on mangrove ecosystem functioning

Upscaling to 0.08 km^2 of tidal channels and pools and 0.75 km^2 of flat area estimated at sites A and B yields

approximately 815 and 161,000 cm^3 of total burrow volume per site, respectively. Based on the drone survey in 2015, we estimated that burrows occupied 0.05 to 30% of the total volume of the mudflat per unit area depending on the habitat considered. The main consequence of increased burrow volume and complexity is the increased extension of surface sediments into deep sediments near channels and depressions, although we did not measure this directly as Agusto et al. (2021) did. This favours the hydrological and biogeochemical fluxes between burrows and overlying waters (Stieglitz et al. 2013), especially when these burrows remain open at high tide. Large complex burrows promote water flow and associated biogeochemical exchanges between sediments and standing water. The type and intensity of these exchanges will depend, however, on the passive or active irrigation of burrows. In the case of passive irrigation, probably prevalent in unactive, large and complex burrows entirely covered by benthic biofilm, only complex burrows with multiple branches promote tidally driven water flow and associated transfer of dissolved components (Ridd 1996; Stieglitz et al. 2000a). These burrows, connected to tidal channels and depressions, may play an important role in removing salts and solutes from reduced sediments (Smith et al. 1991; Stieglitz et al. 2000b) and participate, together with tidal channels, in tidally driven transfers of materials towards the adjacent ecosystems (Mallin and Lewitus 2004; Rezende et al. 2007).

In contrast, single-aperture and simple-shaped burrows not connected to tidal channels and standing water likely play a different role in such a process. During ebb tides, fiddler crabs maintain and leave their burrows for successive short durations. Being unconnected to the tidal channels, these burrows are full of stagnant water during low tide. At high tide, the same burrows, inhabited by crabs, are closed by a sediment plug. Therefore, metabolites locally produced in these burrows could either accumulate in burrows or circulate through the sediment during ebb tides (Xin et al. 2009). Re-oxidation processes of the metabolites are possible within irrigated burrows only (Kristensen 2008). These processes involving non-conservative solutes are, however, not accurately predictable (Aller et al. 2024) because the biogeochemical impacts of burrows vary with species (Aller et al. 1983), burrow sizes and densities (Michaud et al. 2021), but also with the surrounding sediment organic matter reaction rate (Michaud et al. 2010).

Crabs regularly abandon their burrows (Kristensen 2008; Penha-Lopes et al. 2009) which may subsequently be tidally flushed for a number of tidal cycles, given the highly cohesive fine sediments preventing immediate burrow collapse (Needham et al. 2010). Despite their small individual volume, single burrows may thus be hydrologically important given their density.

We observed sediment excavation near small- and medium-sized burrows, highlighting that active burrows are mainly located on the platform. Aschenbroich et al. (2016) calculated that such bioturbation activity could be responsible for the reworking of 91 t day^{-1} km^{-2} during the spring tides in the dry season. In relation with fiddler crab activity, the single-aperture and simple-shaped burrows appear to be associated with more intense sediment reworking than large and complex burrows where we did not observe freshly excavated sediment. The fact that large, complex, inactive burrows are generally connected to tidal channels and depressions suggests that burrow structures can promote the formation/extension of channels and pools by increasing sediment erosion, as has already been observed in salt marshes (Escapa et al. 2015). Such a combined effect of fish and burrowing crabs on sediment drainage has been observed in intertidal salt marshes in Argentina (Perillo et al. 2005). Repetitive water circulation through the multi-species burrows connected to tidal depressions and channels may destabilize and promote the collapsing of their edges, leading to larger depressions. Collapsing abandoned J-shaped fiddler crab burrows may also facilitate passive downward sediment transport and may induce organic matter subduction, modifying diagenetic pathways and processes in sediments (Kristensen 2008; Needham et al. 2010).

Conclusions

The spatial heterogeneity of mud bank geomorphic units is an important controlling factor in the distribution of macrofaunal burrow types and morphologies in pioneer mangroves. The variety of investigated burrow shapes was driven by the presence of tidal depressions and channels. These geomorphic units promoted large and complex burrows and multi-species burrows, presumably leading to a comparatively large volume of ventilated sediment per unit surface area compared to platform areas. While crabs are recognized as the primary macrofauna contributors to the structure and promotion of the microbial mineralization pathways in the biogeochemical mangrove functioning, this study suggests that multiple species associated with burrow construction need to be considered. Depending on their morphology and connectivity with overlying water, burrows may have different functional roles that are likely to induce microhabitat-specific functioning. We must therefore be wary of generalizing ecosystem functioning across geomorphic units where impacts differ according to crab species and abundance, and the flux of reactive organic matter in a given area (among other factors such as the frequency of tidal inundation).

Further studies are needed to understand how different burrow morphologies alter hydrological and biogeochemical functioning. Remineralized solute concentrations in burrow water, in association with reaction rates, and subsequent exchanges with surface water at high tide, may vary with

burrow structure (e.g. Aller et al. 2024). Turnover times of burrow construction and collapse should be assessed in order to evaluate the number of burrows per time unit that will serve as solute accumulators (plugged burrows), as hydrological transfer reactors (un-collapsed open burrows) or as particulate matter transporters and landscape geomorphic shapers (collapsing burrows). Finally, burrow collapse rates relative to burrow volume should be incorporated into the calculation of sediment reworking rates induced indirectly by biological activity.

Supplementary Information The online version contains supplementary material available at https://doi.org/10.1007/s10113-024-02319-z.

Acknowledgements We thank I. Bihannic, A. Alt and J. Printemps for their help in the field, and A. Gardel for providing access to the LEEISA infrastructures and facilities. This paper is a GDR LIGA contribution.

Funding This research was funded by the French National Research Agency (ANR-12-JSV7-0012–01, ANR-10-LABX-19, ANR-13-JCLI-0004) and the "Pépinière Interdisciplinaire de Guyane" (PIG MITI CNRS). RC Aller was supported by NSF grants OCE 1737749, 1332418 and 1060915, and A. Aschenbroich's PhD thesis by the Université de Bretagne Occidentale (UBO).

Data availability Tabulated data not otherwise included in the Supplementary files are available on request from the corresponding author.

References

Agusto LE, Fratini S, Jimenez PJ, Quadros A, Cannicci S (2021) Structural characteristics of crab burrows in Hong Kong mangrove forests and their role in ecosystem engineering. Estuar Coast Shelf Sci 248:106973. https://doi.org/10.1016/j.ecss.2020.106973

Agusto LE, Qin G, Thibodeau B, Tang J, Zhang J, Zhou J, Wu J, Zhang L, Thapa P, Wang F, Cannicci S (2022) Fiddling with the blue carbon: Fiddler crab burrows enhance CO2 and CH4 efflux in saltmarsh. Ecol Ind 144:109538. https://doi.org/10.1016/j.ecolind.2022.109538

Aller RC, Aller JY, Ullman W (1983) Comparative biogeochemistry of water in intertidal Onuphis (polychaeta) and Upogebia (crustacea) burrows: temporal patterns and causes. J Marine Res 571–604. https://elischolar.library.yale.edu/journal_of_marine_research/1695

Aller RC, Klingensmith I, Stieglitz T, Heilbrun C, Waugh S, et al. (2024) Biogeochemical plumbing of pioneer mangrove intertidal flats in French Guiana. Reg Environ Change 24:117. https://doi.org/10.1007/s10113-024-02272-x

Anderson MJ (2017) Permutational multivariate analysis of variance (PERMANOVA). Wiley StatsRef: Statistics Reference Online 1–15. https://doi.org/10.1002/9781118445112.stat07841

Anthony EJ, Gardel A, Gratiot N, Proisy C, Allison M, et al. (2010) The Amazon-influenced muddy coast of South America: a review of mud-bank–shoreline interactions. Earth Sci Rev 103:99–121. https://doi.org/10.1016/j.earscirev.2010.09.008

Araújo JMC, Otero XL, Marques AGB, Nobrega GN, Sylva JRF, et al. (2012) Selective geochemistry of iron in mangrove soils in a semi-arid tropical climate: effects of the burrowing activity of the crabs *Ucides cordatus* and *Uca maracoani*. Geo-Mar Lett 32:289–300. https://doi.org/10.1007/s00367-011-0268-5

Aschenbroich A, Michaud E, Stieglitz T, Fromard F, Gardel A, et al. (2016) Brachyuran crab community structure and associated sediment reworking activities in pioneer and young mangroves of French Guiana, South America. Estuar Coast Shelf Sci 182:60–71. https://doi.org/10.1016/j.ecss.2016.09.003

Austen I, Andersen TJ, Edelvang K (1999) The influence of benthic diatoms and invertebrates on the erodibility of an intertidal mudflat, the Danish Wadden Sea. Estuar Coast Shelf Sci 49:99–111. https://doi.org/10.1006/ecss.1998.0491

Bertness MD, Miller T (1984) The distribution and dynamics of *Uca pugnax* (Smith) burrows in a new England salt marsh. J Exp Mar Biol Ecol 83:211–237. https://doi.org/10.1016/S0022-0981(84)80002-7

Booth JM, Fusi M, Marasco R, Daffonchio D (2023) The microbial landscape in bioturbated mangrove sediment: a resource for promoting nature-based solutions for mangroves. Microb Biotechnol 16:1584–1602. https://doi.org/10.1111/1751-7915.14273

Bortolus A, Iribarne O (1999) Effects of the SW Atlantic burrowing crab *Chasmagnathus granulata* on a Spartina salt marsh. Mar Ecol Prog Ser 178:79–88. https://doi.org/10.3354/meps178079

Brunier G, Fleury J, Anthony EJ, Pottin V, Vella C, et al. (2016) Structure-from-Motion photogrammetry for high-resolution coastal and fluvial geomorphic surveys. Géomorphologie : Relief, Processus, Environnement 22:147–161. https://doi.org/10.4000/geomorphologie.11358

Brunier G, Michaud E, Fleury J, Anthony E, Morvan S, et al. (2020) Assessing the relationship between macro-faunal burrowing activity and mudflat geomorphology from UAV-based Structure-from-Motion photogrammetry. Remote Sens Environ 241:111717. https://doi.org/10.1016/j.rse.2020.111717

Cannicci S, Fusi M, Cimó F, Dahdouh-Guebas F, Fratini S (2018) Interference competition as a key determinant for spatial distribution of mangrove crabs. BMC Ecol 18:8. https://doi.org/10.1186/s12898-018-0164-1

Decho AW (2000) Microbial biofilms in intertidal systems: an overview. Cont Shelf Res 20:1257–1273. https://doi.org/10.1016/S0278-4343(00)00022-4

Dinh QM, Qin JG, Dittmann S, Tran DD (2014) Burrow morphology and utilization of the goby (*Parapocryptes serperaster*) in the Mekong Delta Vietnam. Ichthyol Res 61:332–340. https://doi.org/10.1007/s10228-014-0402-2

Egawa R, Sharma S, Nadaoka K, MacKenzie RA (2021) Burrow dynamics of crabs in subtropical estuarine mangrove forest. Estuar Coast Shelf Sci 252:107244. https://doi.org/10.1016/j.ecss.2021.107244

Escapa M, Perillo GME, Iribarne O (2008) Sediment dynamics modulated by burrowing crab activities in contrasting SW Atlantic intertidal habitats. Estuar Coast Shelf Sci 80:365–373. https://doi.org/10.1016/j.ecss.2008.08.020

Escapa M, Perillo GME, Iribarne O (2015) Biogeomorphically driven salt pan formation in Sarcocornia-dominated salt-marshes. Geomorphology 228:147–157. https://doi.org/10.1016/j.geomorph.2014.08.032

Friess DA, Adame MF, Adams JB, Lovelock CE (2022) Mangrove forests under climate change in a 2°C world. Wires Clim Change 13:e792. https://doi.org/10.1002/wcc.792

Guimond JA, Seyfferth AL, Moffett KB, Michael HA (2020) A physical-biogeochemical mechanism for negative feedback between marsh crabs and carbon storage. Environ Res Lett 15:034024. https://doi.org/10.1088/1748-9326/ab60e2

Henmi Y, Fujiwara C, Kirihara S, Okada Y, Itani G (2017) Burrow morphology of alpheid shrimps: case study of *Alpheus brevicristatus* and a review of the genus. jzoo 34:498–504. https://doi.org/10.2108/zs170055

Karpulus I, Szlep R, Tsurnamal M (1972) Associative behavior of the fish *Cryptocentrus cryptocentrus* (Gobiidae) and the pistol shrimp *Alpheus djiboutensis* (Alpheidae) in artificial burrows. Mar Biol 15:95–104. https://doi.org/10.1007/BF00353637

Katrak G, Dittmann S, Seuront L (2008) Spatial variation in burrow morphology of the mud shore crab *Helograpsus haswellianus* (Brachyura, Grapsidae) in South Australian saltmarshes. Mar Freshwater Res 59:902–911. https://doi.org/10.1071/MF08044

Kristensen E (2008) Mangrove crabs as ecosystem engineers; with emphasis on sediment processes. J Sea Res 59:30–43. https://doi.org/10.1016/j.seares.2007.05.004

Kristensen E, Valdemarsen T, de Moraes PC, Guth AZ, Sumida P, et al. (2022) Pneumatophores and crab burrows increase CO2 and CH4 emission from sediments in two Brazilian fringe mangrove forests. Mar Ecol Prog Ser 698:29–39. https://doi.org/10.3354/meps14153

Lê S, Josse J, Husson F (2008) FactoMineR: an R package for multivariate analysis. J Stat Softw 25:1–18. https://doi.org/10.18637/jss.v025.i01

Li S, Cui B, Xie T, Bai J, Wang Q, et al. (2018) What drives the distribution of crab burrows in different habitats of intertidal salt marshes, Yellow River Delta, China. Ecol Ind 92:99–106. https://doi.org/10.1016/j.ecolind.2017.11.003

Lim S (2006) Fiddler crab burrow morphology: how do burrow dimensions and bioturbative activities compare in sympatric populations of *Uca vocans* (Linnaeus, 1758) and *U. annulipes* (H. Milne Edwards, 1837)? Crustaceana 79:525–540. https://doi.org/10.1163/156854006777584241

Lim S, Diong (2003) Burrow-morphological characters of the fiddler crab, *Uca Annulipes* (h. Milne Edwards, 1837) and ecological correlates in a lagoonal beach on Pulau Hantu. Singapore Crustaceana 76:1055–1069. https://doi.org/10.1163/156854003322753411

Lim SSL, Heng MMS (2007) Mangrove micro-habitat influence on bioturbative activities and burrow morphology of the fiddler crab, *Uca annulipes* (H. Milne Edwards, 1837) (Decapoda, Ocypodidae). Crustaceana 80:31–45

Machado GBO, Gusmão-Junior JBL, Costa TM (2013) Burrow morphology of *Uca uruguayensis* and *Uca leptodactylus* (Decapoda: Ocypodidae) from a subtropical mangrove forest in the western Atlantic. Integr Zool 8:307–314. https://doi.org/10.1111/j.1749-4877.2012.00297.x

Mallin MA, Lewitus AJ (2004) The importance of tidal creek ecosystems. J Exp Mar Biol Ecol 298:145–149. https://doi.org/10.1016/S0022-0981(03)00356-3

Mcleod E, Chmura GL, Bouillon S, Salm R, Bjorks M et al (2011) A blueprint for blue carbon: toward an improved understanding of the role of vegetated coastal habitats in sequestering CO2. Front Ecol Environ 9:552–560. https://doi.org/10.1890/110004

Michaud E, Aller RC, Stora G (2010) Sedimentary organic matter distributions, burrowing activity, and biogeochemical cycling: natural patterns and experimental artifacts. Estuar Coast Shelf Sci 90:21–34. https://doi.org/10.1016/j.ecss.2010.08.005

Michaud E, Aller RC, Zhu Q, Heilbrun C, Stora G (2021) Density and size-dependent bioturbation effects of the infaunal polychaete Nephtys incisa on sediment biogeochemistry and solute exchange. J Mar Res 79:181–220. https://doi.org/10.1357/002224021834670801

Michaud E, Aschenbroich A, Gauthier O, Fromard F, Aller J et al (2022) The codevelopment of mangroves and infaunal community diversity in response to the natural dynamics of mud deposition in French Guiana. Sustainability 14:2829. https://doi.org/10.3390/su14052829

Min WW, Kathiresan K (2021) Burrow morphologies, crab characteristics and soil properties in different seasons across intertidal areas of a restored mangrove forest. J Sea Res 177:102111. https://doi.org/10.1016/j.seares.2021.102111

Morrisey DJ, DeWitt TH, Roper DS, Williamson RB (1999) Variation in the depth and morphology of burrows of the mud crab *Helice crassa* among different types of intertidal sediment in New Zealand. Mar Ecol Prog Ser 182:231–242. https://doi.org/10.3354/meps182231

Needham HR, Pilditch CA, Lohrer AM, Thrush SF (2010) Habitat dependence in the functional traits of *Austrohelice crassa*, a key bioturbating species. Mar Ecol Prog Ser 414:179–193. https://doi.org/10.3354/meps08726

Needham HR, Pilditch CA, Lohrer AM, Thrush SF (2013) Density and habitat dependent effects of crab burrows on sediment erodibility. J Sea Res 76:94–104. https://doi.org/10.1016/j.seares.2012.12.004

Needham HR, Pilditch CA, Lohrer AM, Thrush SF (2011) Context-specific bioturbation mediates changes to ecosystem functioning. Ecosystems 14:1096–1109. https://doi.org/10.1007/s10021-011-9468-0

Nie L, Li Y, Hou Y, Di L, Xi M, et al. (2021) Dynamics of organic carbon under bioturbation by mud crabs (*Macrophthalmus japonicus*) and clamworms (*Perinereis aibuhitensis*) in an estuary ecosystem. J Exp Mar Biol Ecol 534:151474. https://doi.org/10.1016/j.jembe.2020.151474

Oksanen J, Blanchet FG, Friendly M, Kind R, Legendre P et al (2020) Vegan: community ecology package. R package version 2.5–7. https://CRAN.R-project.org/package=vegan

Penha-Lopes G, Bartolini F, Limbu S, Cannicci S, Kristensen E, et al. (2009) Are fiddler crabs potentially useful ecosystem engineers in mangrove wastewater wetlands? Mar Pollut Bull 58:1694–1703. https://doi.org/10.1016/j.marpolbul.2009.06.015

Perillo GME, Minkoff DR, Piccolo MC (2005) Novel mechanism of stream formation in coastal wetlands by crab–fish–groundwater interaction. Geo-Mar Lett 25:214–220. https://doi.org/10.1007/s00367-005-0209-2

Proisy C, Gratiot N, Anthony EJ, Gardel A, Fromard F, et al. (2009) Mud bank colonization by opportunistic mangroves: a case study from French Guiana using lidar data. Cont Shelf Res 29:632–641. https://doi.org/10.1016/j.csr.2008.09.017

Qureshi NA, Saher NU (2012) Burrow morphology of three species of fiddler crab (Uca) along the coast of Pakistan. Belg J Zool 142:114–126. https://doi.org/10.26496/bjz.2012.152

R Development Core Team (2021) R: A language and environment for statistical computing. Available online: https://www.gbif.org/tool/81287/r-alanguage-and-environment-for-statistical-computing. Accessed 7 Oct 2021

Rezende CE, Lacerda LD, Ovalle ARC, Silva LFF (2007) Dial organic carbon fluctuations in a mangrove tidal creek in Sepetiba bay, Southeast Brazil. Braz J Biol 67:673–680. https://doi.org/10.1590/S1519-69842007000400012

Ridd PV (1996) Flow through animal burrows in mangrove creeks. Estuar Coast Shelf Sci 43:617–625. https://doi.org/10.1006/ecss.1996.0091

Smith TJ, Boto KG, Frusher SD, Giddins RL (1991) Keystone species and mangrove forest dynamics: the influence of burrowing by crabs on soil nutrient status and forest productivity. Estuar Coast

Shelf Sci 33:419–432. https://doi.org/10.1016/0272-7714(91)90081-L

Stieglitz T, Ridd P, Müller P (2000a) Passive irrigation and functional morphology of crustacean burrows in a tropical mangrove swamp. Hydrobiologia 421:69–76. https://doi.org/10.1023/A:1003925502665

Stieglitz T, Ridd PV, Hollins S (2000b) A small sensor for detecting animal burrows and monitoring burrow water conductivity. Wetlands Ecol Manage 8:1–7. https://doi.org/10.1023/A:1008441400602

Stieglitz TC, Clark JF, Hancock GJ (2013) The mangrove pump: the tidal flushing of animal burrows in a tropical mangrove forest determined from radionuclide budgets. Geochim Cosmochim Acta 102:12–22. https://doi.org/10.1016/j.gca.2012.10.033

Underwood AJ, Chapman MG, Crowe TP (2004) Identifying and understanding ecological preferences for habitat or prey. J Exp Mar Biol Ecol 300:161–187. https://doi.org/10.1016/j.jembe.2003.12.006

Wang J, Tang L, Zhang X, Wang C, Gao Y et al (2009) Fine-scale environmental heterogeneities of tidal creeks affect distribution of crab burrows in a Chinese salt marsh. Ecol Eng 35:1685–1692. https://doi.org/10.1016/j.ecoleng.2009.05.002

Wang M, Gao X, Wang W (2014) Differences in burrow morphology of crabs between *Spartina alterniflora* marsh and mangrove habitats. Ecol Eng 69:213–219. https://doi.org/10.1016/j.ecoleng.2014.03.096

Wunderlich AC, Pinheiro MA (2013) Mangrove habitat partitioning by *Ucides cordatus* (Ucididae): effects of the degree of tidal flooding and tree-species composition during its life cycle. Helgol Mar Res 67:279–289. https://doi.org/10.1007/s10152-012-0322-3

Xi M, Zhang Q, Nie L, Xiong T, Yu Z (2023) Quantitative comparison of clamworm (*Perinereis aibuhitensis*) and crab (*Macrophthalmus japonicus*) burrowing effects on nitrogen and phosphorus dynamics at the sediment–water interface. Sci Total Environ 857:159559. https://doi.org/10.1016/j.scitotenv.2022.159559

Xin P, Jin G, Li L, Barry DA (2009) Effects of crab burrows on pore water flows in salt marshes. Adv Water Resour 32:439–449. https://doi.org/10.1016/j.advwatres.2008.12.008

Authors and Affiliations

Emma Michaud[1] · Adelaide Aschenbroich[1] · Thomas Stieglitz[2,3] · Guillaume Brunier[2,4] · Robert Curwood Aller[5] · Edward Anthony[2] · François Fromard[6] · Gérard Thouzeau[1]

✉ Emma Michaud
emma.michaud@univ-brest.fr

Adelaide Aschenbroich
adelaide.aschenbroich@gmail.com

Thomas Stieglitz
thomas.stieglitz@ird.fr

Guillaume Brunier
g.brunier@brgm.fr

Robert Curwood Aller
robert.aller@stonybrook.edu

Edward Anthony
anthony@cerege.fr

François Fromard
francois.fromard@univ-tlse3.fr

Gérard Thouzeau
gerard.thouzeau@univ-brest.fr

[1] Univ Brest, CNRS, IRD, Ifremer, LEMAR, 29280 Plouzane, France

[2] Aix Marseille Univ, CNRS, IRD, INRAE, CEREGE, 13 545, Aix-en-Provence, France

[3] Centre for Tropical Water and Aquatic Ecosystem Research (TropWATER), James Cook University, Townsville, QLD 4811, Australia

[4] French Geological Survey, BRGM, 97 300 Cayenne, French Guiana

[5] School of Marine and Atmospheric Sciences, Stony Brook University, New York, NY 11794-5000, USA

[6] Laboratoire Ecologie Fonctionnelle Et Environnement, Université de Toulouse, CNRS, INP, 31 062 Toulouse, France